Hindawi
Shock and Vibration
Volume 2018, Article ID 4276167, 18 pages
https://doi.org/10.1155/2018/4276167

Research Article

Seismic Response of the Three-Span Bridge with Innovative Materials Including Fault-Rupture Effect

Jiping Ge [1,2] **and M. Saiid Saiidi** [2]

[1] *School of Urban Construction and Safety Engineering, Shanghai Institute of Technology, Shanghai 201418, China*
[2] *Department of Civil and Environmental Engineering, University of Nevada, Reno, NV 89557, USA*

Correspondence should be addressed to Jiping Ge; bridgejiping@126.com

Received 23 November 2017; Revised 3 May 2018; Accepted 13 May 2018; Published 9 July 2018

Academic Editor: Carlo Trigona

The seismic performance of the SR99 Bridge with conventional and advanced details in Seattle, Washington, was studied via a nonlinear, time history analysis of a multidegree of freedom model. The bridge consists of three spans supported on two single-column piers and will be the first built bridge in the world in which superelastic shape memory alloy (SMA) and engineered cementitious composite (ECC) are implemented to reduce damage at plastic hinges and minimize residual displacements. Existing finite-element formulations in the finite-element software OpenSees are used to capture the response of the advanced materials used in the bridge. The earthquake induced by strike-slip fault was assumed to produce a surface rupture across the SR99 Bridge. The effect of the rupture was modeled by a static, differential ground displacement in the fault-parallel direction across the rupture. The synthetic suite of scaled bidirectional near-fault ground motions used in the analysis contains common near-fault features including a directivity pulse in the fault-normal direction and a fling step in the fault-parallel direction. Comparisons are made on behavior of two different bridge types. The first is a conventional reinforced concrete bridge and the second is a bridge with Nickel-Titanium (NiTi) SMA reinforcing bar at the plastic hinge zone and ECC in the whole column. Fault-parallel near-fault earthquakes typically exhibit a static permanent ground displacement caused by the relative movement of the two sides of the fault. When the fault is located between piers, the pier shows a higher demand. Fault-normal analysis results show effectiveness of the innovative interventions on the bridges in providing excellent recentering capabilities with minimal damage to the columns. But the maximum drift computed in the SMA bridge is slightly higher than reinforced concrete (RC) bridges, contributed by comparatively low stiffness of the superelastic SMA bars compared to the steel reinforcing bars.

1. Introduction

Experience with recent earthquakes, such as the Kocaeli and Duzce earthquakes and the 1999 Chi-chi Earthquake in Taiwan, shows that all bridges built close to known faults must have greater displacement capacities than those designed for far-field ground motions. However, existing seismic design strategies for bridges are largely based on design ground motions without near-fault characteristics and do not provide guidance for designing bridges near active faults [1–3].

The Bolu Viaduct, which was essentially complete (except for installation of expansion joints) when it was hit by the Duzce earthquake (Mw = 7.2), in Turkey in 1999. The North Anatolian Fault zone is the most prominent and active strike-slip-type fault running across northern Turkey with an approximate length of 1300km and a slip rate of 25 mm/yr. A postearthquake investigation at the viaduct site revealed that the fault crosses the viaduct (between Piers P44 and P45) at an angle of about 25°, and the ground dislocation in the fault-parallel direction across the rupture was approximately 1.5 m (59.1 in.). In the analysis by Park et al. (2004), two different ground motions, each involving a static slip of 0.75 m (29.55 in.) in opposite directions, were imposed upon the two sides of the ground separated by the surface rupture, resulting in a net ground dislocation of 1.5 m. Results revealed that the static ground displacement had to be accounted for in the dynamic analysis in order to achieve the observed performance. The study asserts that all bridges built close to known faults must

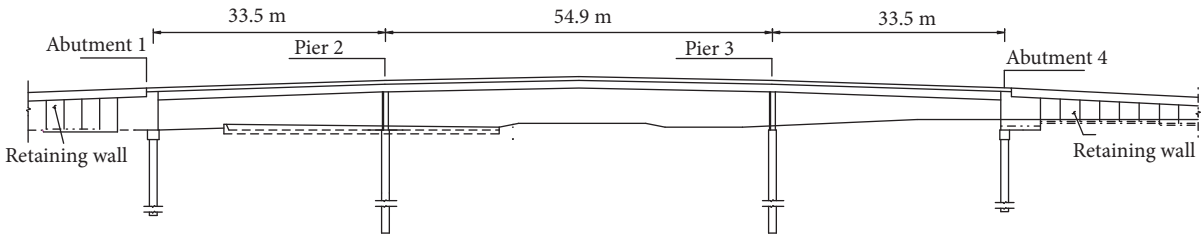

Figure 1: Demonstration project bridge elevation.

have greater displacement capacities than those designed for far-field ground motions [4, 5].

Choi et al. (2007) studied the effect of fault-rupture [6]. A quarter-scale reinforced concrete bridge model was subjected to a series of incoherent ground motions that simulated fault-rupture. The bridge model was subjected to six earthquake runs until one of the shake tables reached its displacement limit. During this run, some of the bridge columns approached failure but there was no steel bar rupture. The measured data showed a major shift in the location of the most critical pier compared to an identical bridge mode that had been subjected to uniform motion [7]. The pier that was the least damaged under uniform ground motion suffered the largest damage in the case of shaking that simulated fault-rupture.

Previous research and experience demonstrate that superelastic shape memory alloy (SMA) and engineered cementitious composite (ECC) have promising performance in minimizing damage and residual deformations. Wang and Saiidi were the first researchers to utilize SMA bars as reinforcement in RC structures [8, 9]. They studied the seismic performance of reinforced concrete columns detailed with SMA bars at the plastic hinge zone, showing that residual deformations were insignificant, thus requiring minimal repair. The particular feature that is of interest in the current study is the superelastic effect and the ability for the SMA to deform but recover the deformation upon removing of the applied load. The superelastic capability of SMAs is attractive because it can help minimize permanent deformations in structures where residual drift caused by large earthquakes is a concern. There are many types of SMA alloys. Among those alloys, Nickel and Titanium (NiTi) SMA has gained more attention since it exhibits a large superelastic strain recovery, high energy dissipation, excellent low- and high-cycle fatigue properties, and excellent corrosion resistance [10]. Because of these properties, only NiTi SMA was considered in the present study.

ECC is a highly ductile, durable, and sustainable material. ECC has the ability to reach the ultimate tensile strain of approximately 3% to 5%. This high strain capacity (nearly 500 times larger than that of conventional concrete) is due to the strain hardening behavior and unique cracking mechanism of ECC [11]. Cruz and Saiidi (2012) used advanced materials and details to minimize the earthquake damage and residual deformations in a quarter-scale, four-span bridge model subjected to strong shake table seismic excitations [12]. One of the different innovative column designs incorporated superelastic SMA reinforcing bars with ECC concrete in the plastic hinge region. Cruz and Saiidi (2013) reported that the earthquake damage in the plastic hinge regions of the columns detailed with innovative materials was minimal and that residual drift in the bridge piers was insignificant [13].

The superelastic SMA material has ability to undergo large strains (up to 8%) and still recover its shape through stress removal. The ECC material can enhance ductility due to its high tensile strain capacity. The combination of the high tensile strain capacity of ECC with the superelastic characteristics of the SMA material offers the potential of increasing ductility, while decreasing damage and residual displacement under cyclic loads. So SMA and ECC are being implemented by the Washington State Department of Transportation (WashDOT) in the construction of the SR99 off-ramp bridge in Seattle, Washington, as a demonstration project funded by the United States Federal Highway Administration. The bridge consists of three spans supported on two single-column piers. This will be the first built bridge in the world in which SMA and ECC are implemented to improve the seismic performance. Due to the uniqueness of these columns, analytical modeling was conducted to assess the performance and provide design recommendations for full scale columns [14]. It is not clear how the combination of SMA/ECC would affect the response of the bridge, especially when a presently unknown fault crosses this bridge.

The primary objective of the paper is to study the seismic response of three-span bridges with innovative materials under a near-fault ground motion with incoherent motions that included the fault-rupture effect. The research aims to increase the understanding of the fault-rupture effects on the seismic response of the bridge system that cross active faults through dynamic analysis and how individual bridge components interact within a bridge system. The main goals pursued in this study are to determine any beneficial effects of incorporating SMA and ECC details at critical zones of the columns of the innovative bridge in improving its seismic performance in terms of damage and residual displacements.

2. Description of the Bridge

2.1. Bridge Properties. The SR-99 Northbound off-ramp bridge is a three-span continuous box-girder structure with two pier shaft columns and integral abutments, as shown in Figure 1. The superstructure consists of two, 1.83 m deep prestressed precast concrete box girders, and spaced 4.65

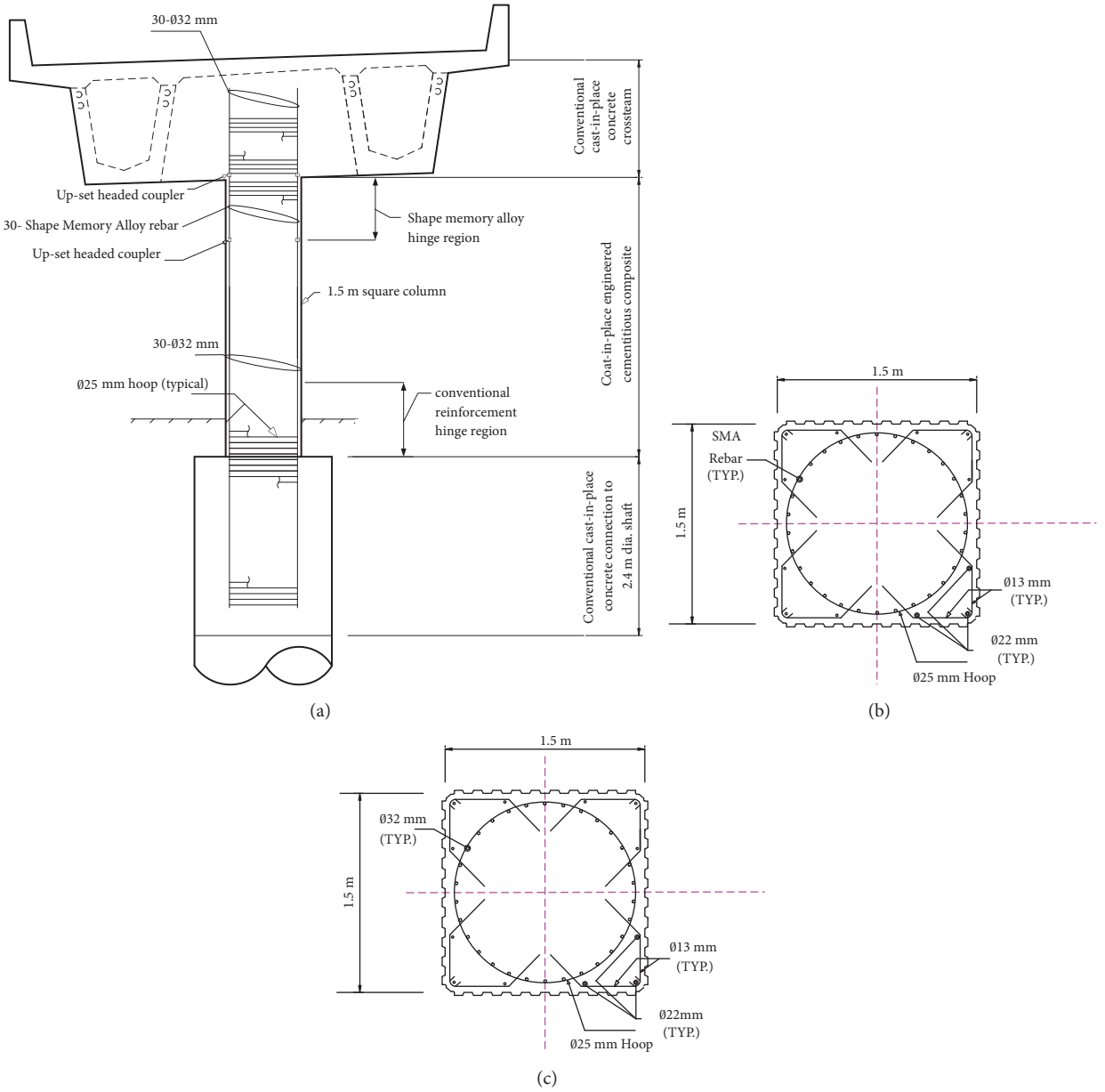

Figure 2: SR99 pier elevation column cross section details: (a) pier elevation, (b) SMA section, and (c) mild steel section.

m on center. The roadway is a 20.32 cm thick cast-in-place concrete slab with a total width of 9.30m. The intermediate piers are constructed from 1.83 m deep by 2.13 m wide integral cast-in-place concrete cap beams supported by single 1.52 by 1.52 m cast-in-place concrete columns. The heights of the intermediate piers are 5.18 m and 5.87 m, for Pier 2 and Pier 3, respectively, measured from the top of the pile cap to the bottom of the cap beam. The column cross section is square with longitudinal reinforcement placed in a circular pattern and spiral lateral reinforcement, forming a circular core (Figure 2). There is additional longitudinal reinforcement in the corners, which is provided for architectural reasons.

The top of the columns is a moment connection with 30-#10 (30-Ø32mm) SMA bars, for a longitudinal reinforcement ratio of 1.0%. The SMA bars are connected to 30-#10 mild steel reinforcing bars using headed couplers. The couplers are stronger than the bars and they force failure in the bars rather than the coupler. The SMA bars are used only at the top plastic hinges because preliminary analysis by the bridge designers indicated that top plastic hinges were more critical than bottom plastic hinges. The length of the SMA bars is 1.22 m, measured from the column-girder interface to the lower couplers. ECC is used over the upper 1.52 m (100% of the column side dimension) of the column clear height. The transverse reinforcement is #8 (Ø25 mm) butt-welded hoops spaced at 10.2 cm. Each column is supported by a single 2.44 m diameter C cast-in-place shaft. The abutments are supported by 2 identical 1.98 m diameter piles in a single row, spaced 6.10 m on centers.

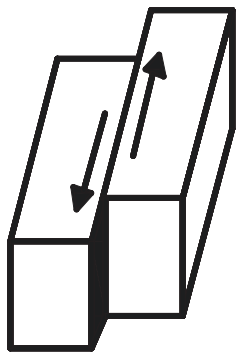

Figure 3: Strike-slip fault.

2.2. Near-Fault Ground Motions. Near-fault ground motions usually contain both intense dynamic motions and large static displacements. The intense, coherent dynamic motions are caused by forward rupture directivity that is commonly characterized by a long-period velocity pulse acting normal to the fault. This pulse is usually narrow-band and is reflected in the response spectrum by a peak occurring approximately at the period of this pulse. The period of a directivity pulse has been reported to increase with the magnitude of the earthquake.

Static ground displacements in near-fault ground motions are caused by one rock bed slipping toward another rock bed, on which the earthquake takes place; see Figure 3. If there is faulting at the ground surface, the ground displacement is discontinuous across the surface fault-rupture and can subject a bridge crossing the fault to significant differential movements, posing potentially a major seismic hazard. Coherent dynamic motions in the fault-normal direction and permanent static displacements in the fault-parallel direction occur almost simultaneously and thus these two effects are treated as coincident.

The motions used in the present study are the same as those used by Hoon Choi [2] and Somerville P. G. [15, 16]. The fault-parallel and fault-normal components of simulated acceleration motions are shown in Figure 4. The displacement history of fault-parallel components obtained through a double integration of the acceleration history in Figure 5(a). It can be seen that there is a permanent ground displacement in the fault-parallel direction. Approximately 0.75 m of permanent ground displacement is generated between two piers crossing the fault for the prototype. As mentioned above, the magnitude of the ground dislocation in the fault-parallel direction across the rupture was approximately 1.5 m for Bolu Viaduct and that is double the displacement magnitude of the motions of Figure 5(a). Greater excitations were considered in the present study by increasing the displacements shown in Figure 5. In Figure 5(b), the ground motion record contains near-fault features including a pronounced directivity velocity pulse in the fault-normal component. In order to ensure kinematic continuity in the fault-normal direction, the same fault-normal component is applied to both sides of the surface rupture.

Differential ground movements across the fault-rupture is included in the analysis. For example, in Figure 6, slippage takes place in the north-south direction. When the fault is located in the middle of the piers, different ground motions are assigned to different abutments and piers.

3. Analytical Model

This section first presents a general description of the analytical model of the two cases of the bridge and modeling assumptions for the bridge piers, the abutments, and the foundation and then presents a capacity analysis of the bridges. A global view of the model is presented in Figure 7, where the X-axis is the longitudinal direction of the bridge, the Y-axis is the transverse direction, and the Z-axis is vertical. The model was built in OpenSees [17], which is an open source structural analysis software for nonlinear dynamic analysis.

The bridge superstructure is represented by a spine model using four elastic frame elements for each of the side spans and six elastic frame elements for the middle span. At each pier, the superstructure is tied to the cap through an assemblage of rigid link elements. The material model is very important in the nonlinear finite-element analysis. The detail of all the nonlinear material models of the concrete, reinforcement, and SMA used in the dynamic analysis can be found in [18].

The fiber sections of the columns were created in Xtract [19] and exported to OpenSees. Xtract had to be used because the fiber patch commands in OpenSees do not have the ability to create a circular mesh inside a square to represent the columns in the SR99 Bridge. Figure 8 shows the fiber section used in modeling SR99-RC and SR99-SMA/ECC. The soil properties are simulated with the p-y model, which is a predefined model to describe the nonlinear response of piles in software OpenSees [17].

Longitudinal bars slippage relative to the surrounding concrete when stressed under tensile forces is known as the bond slip effect also known as strain penetration. The slippage usually affects the local and global response of RC members. The cumulative strain difference between the bar and concrete causes a slip at the loaded end of the anchored bar. Consequently, a crack forms and an end rotation occurs adding to the flexural rotation of the member at the connection interface. Studies have indicated that bond slip rotation at the column-footing interface can account for as much as 15-20% of the lateral displacement of a column [20]. Thus it is critical to account for this behavior when developing analytical models.

A zero length element, referred to as "ZeroLengthSection", was used in modeling the bond slip effect in SR99-RC. For the zero length section the mild steel bars were modeled using the material "Bond_SP01". Bond slip did not need to be considered in SR99-SMA/ECC due to the couplers acting as mechanical anchors at a shallow depth in the cap beam. Mechanical anchors tend to substantially decrease bond slip.

4. Bridge Seismic Response

Near-fault ground motions often contain permanent ground displacements. These ground displacements are caused by the

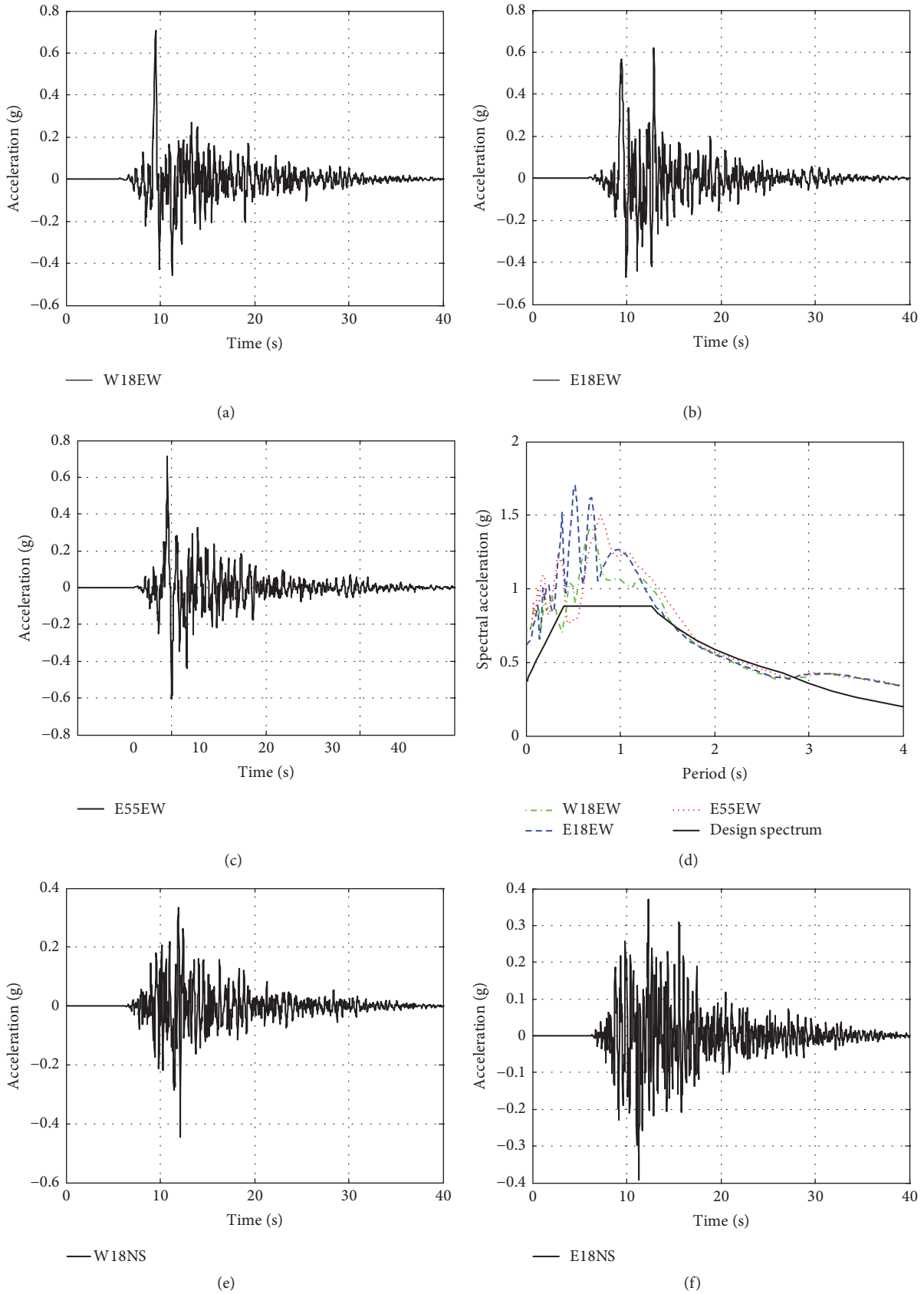

Figure 4: Continued.

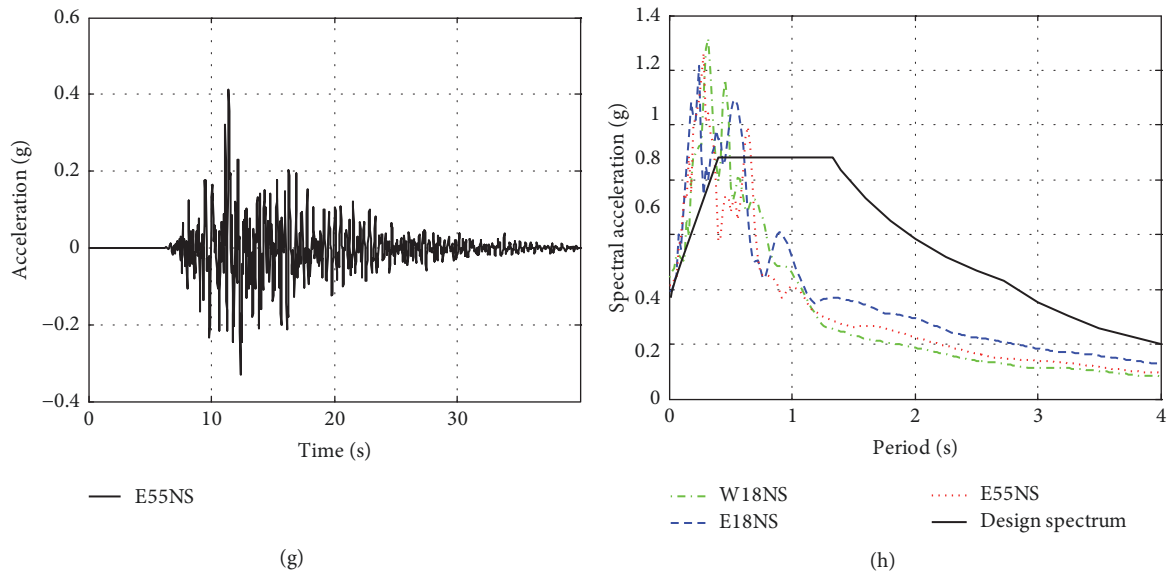

Figure 4: Time history of acceleration: (a) W18EW, (b) E18EW, (c) E55EW, (d) response spectrum in the EW direction, (e) W18NS, (f)E18 NS, (g) E55 NS, and (h) response spectrum in the EW direction.

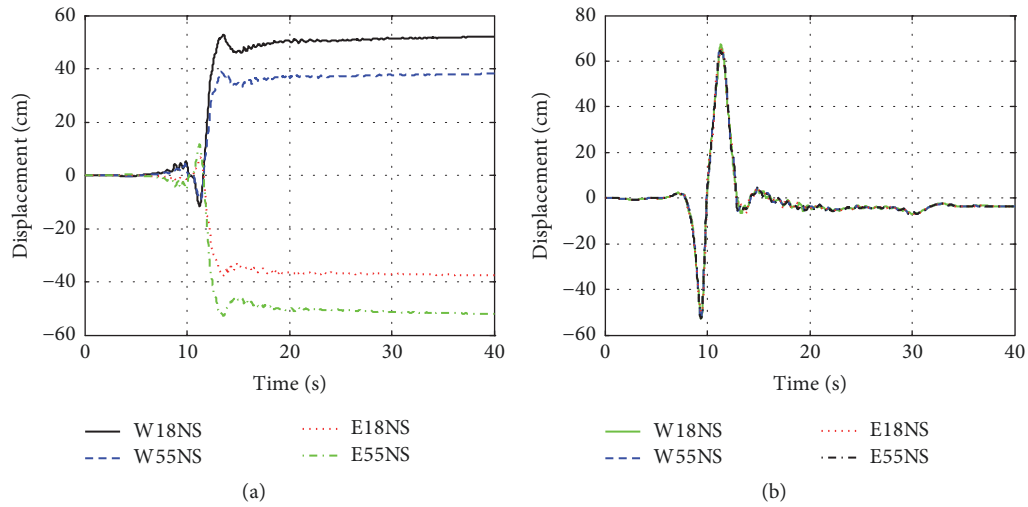

Figure 5: Simulated ground displacement: (a) parallel to the fault and (b) normal to the fault.

relative movement of the two sides of the fault in having surface rupture and can subject a bridge crossing a fault to significant differential displacements. These static ground displacements occur at about the same time as the large dynamic motions, indicating that the static and dynamic displacements need to be treated as coincident loads.

The purpose of this study is to investigate the fault-rupture effects on the seismic response of a bridge system that crosses an active fault. To accomplish the objective of the study, two bridge models are subjected to series of incoherent ground motions that include the fault-rupture effects. The response of these two bridges is compared with the response of the same bridge models subjected to uniform transverse motions. The input records combinations are 'the dead load + the transverse excitation' and 'the dead load + the longitudinal excitation' separately.

4.1. Response under Uniform Excitation. The SR99-RC and SR99-SMA/ECC were analyzed under several uniform excitations in the transverse and longitudinal direction of the bridge. The graphs of the input acceleration records are shown in Figure 4.

Figure 9 shows the base shear versus drift hysteresis curves in the transverse direction. The hysteresis plots were comparatively stable. For smaller displacement demand compared to the design suite ground motion, there is effective recentering mechanism in the SMA bridge and the RC bridge. The corresponding maximum column displacements in the transverse direction are listed in Table 1. It is seen that the E55 motion is the most demanding of all three motions since it causes the largest pier maximum displacements, varying from 1.88 % in the SMA model to 1.70% in the RC model.

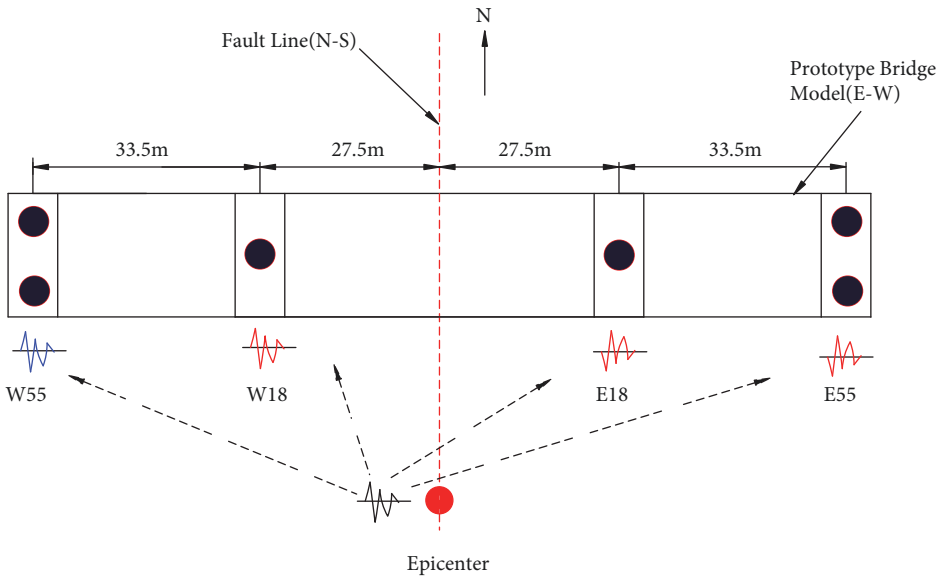

Figure 6: Bridge and fault locations for ground motion simulation.

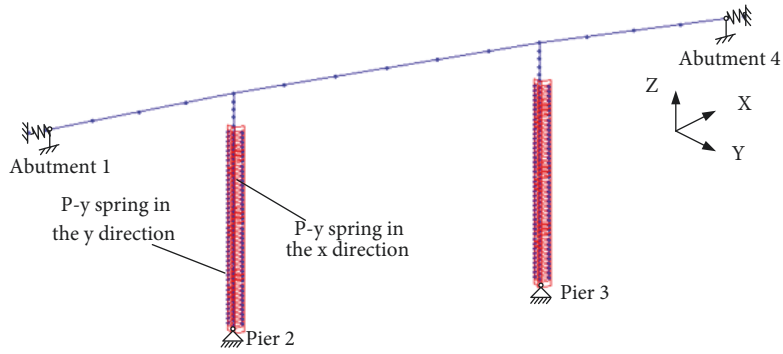

Figure 7: Global view of the bridge model.

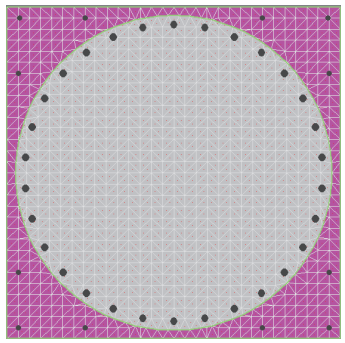

Figure 8: Fiber section of the columns.

For the same level of excitation, the SMA column has the bigger maximum displacement than the RC column. The motion intensity is very small causing maximum drift ratios of 1.88%. Hysteresis response and recentering cannot be judged based on such a small motions. So the amplitude of each motion is double scaled to produce a bigger peak drift. This analysis was repeated using the much stronger ground motion. It is seen that the E55 motion is the most demanding of all three motions since it causes the largest pier maximum displacements, varying from 4.98 % in the SMA model to 4.20% in the RC model. For the same level of excitation, the SMA column still has the bigger maximum displacement than the RC column.

The results in the longitudinal direction are shown in Table 2. It is seen that the W18 motion is the most demanding of all three motions since it causes the largest pier maximum displacements, varying from 3.25 % in the SMA model to 2.40% in the RC model. For the same level of excitation, the SMA column has the bigger maximum displacement than the RC column. Since the ground motions did not produce significant residual displacement with full amplified motions under acceleration and displacement excitation, the amplitude of each motion was scaled to double amplified motions. The goal of this analysis was to see the residual drift of the columns. This analysis is representative of dynamic increase analysis where the amplitude is generally increased to levels much higher than the design earthquake. From

Table 1: Results in the transverse direction under uniform excitation.

Motion	PGA(g)	Model	Peak drift(%)	Double peak drift(%)
W18	0.325	SMA	1.31	3.00
		RC	1.23	2.69
E18	0.387	SMA	1.31	3.41
		RC	1.23	2.96
E55&W55	0.375	SMA	1.88	4.98
		RC	1.70	4.20

Table 2: Results in the longitudinal direction under uniform excitation.

Motion	PGA(g)	Model	Peak Drift(%)	Double Peak Drift(%)
W18	0.325	SMA	3.25	7.37
		RC	2.40	5.90
E18	0.387	SMA	2.20	8.59
		RC	1.86	7.28
E55&W55	0.375	SMA	2.68	11.57
		RC	2.38	10.85

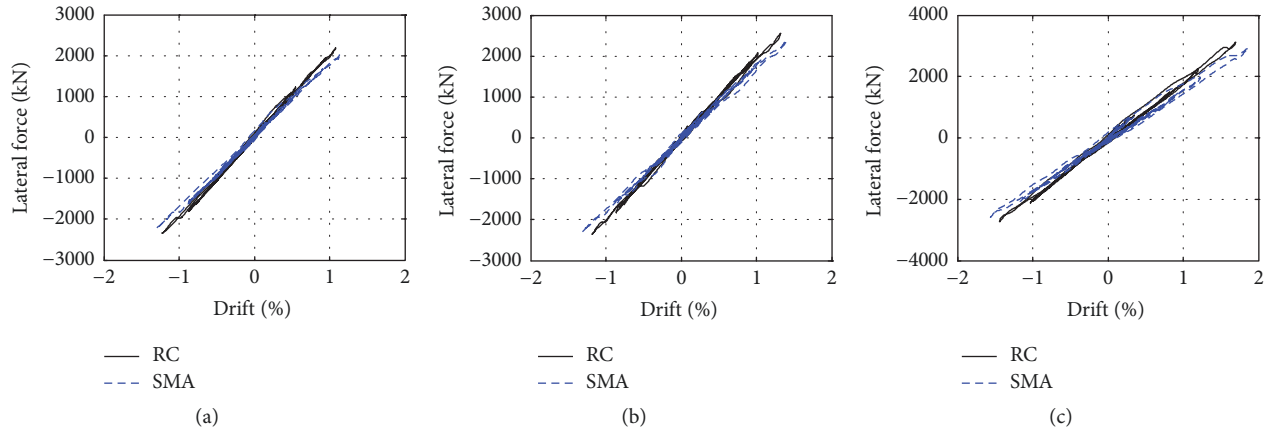

Figure 9: Force displacement hysteresis of the column: (a) W18 synthetic motion, (b) E18 synthetic motion, and (c) E55 synthetic motion.

Table 2, it is seen that the E55 motion is the most demanding of all three motions since it causes the largest pier maximum displacements, varying from 11.57 % in the SMA model to 10.85% in the RC model. For the same level of excitation, the SMA column has the bigger maximum displacement than the RC column. Figures 10(a) and 10(d) show the base shear versus drift hysteresis curves with full amplified W18 motions and double amplified W18 motions. The bridge with SMA column had the bigger maximum displacement than the bridge with RC column. Figures 10(b) and 10(e) show relative drift of piers. Overall, it is seen that the time history shape are nearly the same, but the amplitude of the drift is quite different. Figures 10(c) and 10(f) show the top displacement history of pier. Both the shape and the amplitude of the top displacement under the acceleration excitation are close.

4.2. Fault-Rupture in the Transverse Direction. The analysis of the bridge models using OpenSees is conducted for three different cases having different fault locations (Figure 11) to understand the basic behavior of the model for each case. This is because at this time location of earthquake faults at the site of Bridge SR99 is not known.

The calculated displacement histories for Pier 2 and Pier 3 are plotted in Figure 12. The most distinct measured column response is the relatively high magnitude of residual displacements even under moderate levels of motion. The analyzed data in the fault-rupture study shows a major shift in the location of the pier compared to the bridge that is subjected to fault-rupture motions. The RC column has smaller residual displacement demands compared with the SMA model because it is stiffer than the SMA model.

The cumulative area of the hysteresis loops represents the total energy dissipated through the inelastic mechanism. Figure 13 shows accumulated force displacement hysteresis relationships. The calculated force displacement curves for Pier 2 and Pier 3 show similar shape for the two kinds of

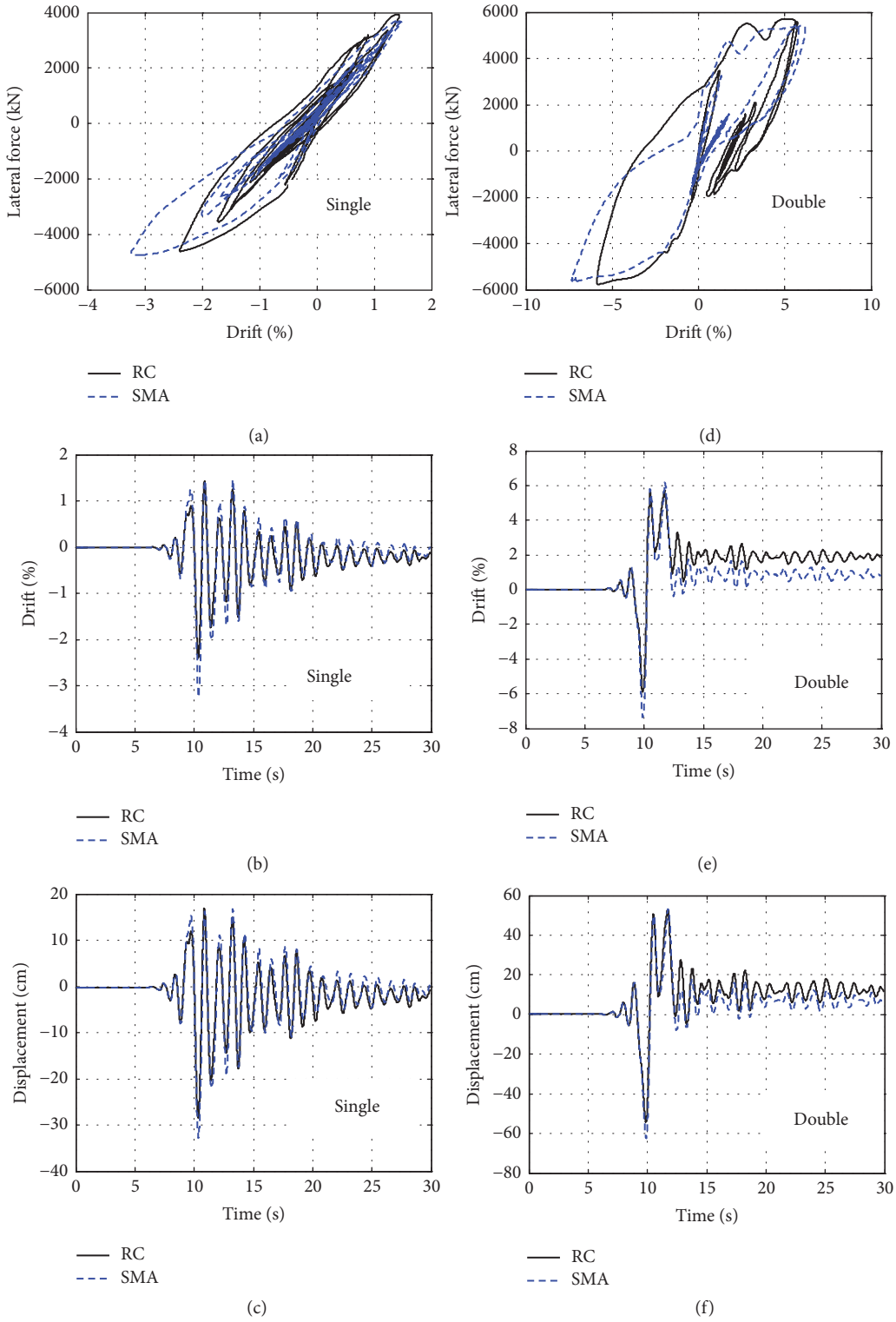

FIGURE 10: The response of the Pier 3 under longitudinal acceleration excitation: (a) and (d) base shear versus drift hysteresis curves, (b) and (e) relative drift of piers, and (c) and (f) top displacement history of piers.

Table 3: Peak drift results of fault-rupture study in the transverse direction (%).

Case	Fault location	Model	Peak drift(%) Pier2/Pier3	Double input peak drift(%) Pier2/Pier3
Case 1	Abut.1 and Pier 2	SMA	2.42/0.69	6.75/1.92
		RC	2.27/0.65	5.74/1.71
Case 2	Pier2 and Pier3	SMA	1.14/1.72	2.05/4.61
		RC	1.07/1.61	2.01/4.24
Case 3	Pier3 and Abut.4	SMA	0.67/2.81	1.97/8.21
		RC	0.63/2.52	1.80/7.72

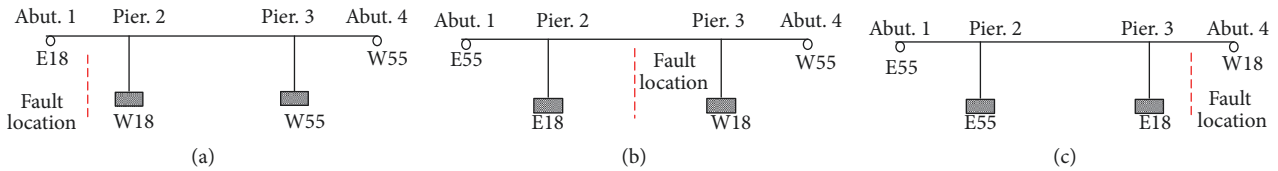

Figure 11: Different cases for fault location: (a) Case 1, (b) Case 2, and (c) Case 3.

bridges. The RC column has smaller displacement demands compared with the SMA model.

The key responses of the model for three cases are listed in Table 3. For Case 1 and Case 3, the pier near the fault has significant peak drift demands. For Case 2, the seismic responses for fault-rupture motions result in bigger demands on bridge columns in Pier 2 than Pier 3, because Pier 2 is higher than Pier 3. It can be seen that the location of fault-rupture also can be a determining factor.

Since the ground motions do not produce significant deformation demand in the columns and the amplitude of each motion is double scaled to produce a bigger peak drift. This presents a much stronger near-fault ground motion will hit the SR99 Bridge in the potential earthquake. The goal of this analysis is to see the residual drift of the columns when double amplified ground motion. This analysis is representative of dynamic increase analysis where the amplitude is generally increased to levels much higher than the design earthquake.

The calculated displacement histories for each pier are plotted in Figure 14. It shows a major shift in the location of the pier compared to the bridge that is subjected to nonuniform motion. Figure 15 shows the base shear versus drift hysteresis curves for selected excitation. It is hard to distinguish which one has dissipated more energy for RC bridge and SMA bridge, because the shift move is dominant instead of cyclic vibration. The corresponding maximum column displacements are also listed in Table 3. It is seen that Case 3 is the most demanding of all three cases since it causes the largest pier maximum displacements and permanent deformations, varying from 8.44% in the SMA model to 8.09% in the RC model. The RC column has smaller residual displacement demands compared with the SMA model because of the smaller stiffness of the SMA model.

4.3. Fault-Rupture in the Longitudinal Direction. The response in the longitudinal direction is dominant by motion of the fault-normal direction; the same fault-normal component is applied to both sides of the surface rupture.

Figures 16(a) and 16(b) show the base shear versus drift hysteresis curves of Pier 2 and Pier 3. There is effective recentering mechanism in both SMA bridge and the RC bridge. Figures 16(c) and 16(d) show relative drift of Pier 2 and Pier 3. Overall, it is seen that the wave shape of Pier 2 and Pier 3 is nearly the same, and the magnitude of Pier 2 is nearly double Pier 3. Figures 16(e) and 16(f) show the top displacement history of Pier 2 and Pier 3. The top displacement history of Pier 2 and Pier 3 is the same. They moved in-phase with slight residual displacements.

In order to simulate a static, differential ground displacement of 1.5m in the fault-parallel direction, a separate fault-parallel component of the ground motion, generated in a similar manner except for using a reversed fling step that affects a static ground displacement of 0.75m in the opposite direction, is applied to the ground on the opposite side of the surface rupture (see Figure 4). Figures 17(a) and 17(b) show the base shear versus drift hysteresis curves of Pier 2 and Pier 3. There is effective recentering mechanism in both SMA bridge and the RC bridge. Figures 17(c) and 17(d) show relative drift of Pier 2 and Pier 3. It is seen that the wave shape of Pier 2 and Pier 3 is nearly the same, and the magnitude of Pier 2 is nearly double Pier 3. Figures 17(e) and 17(f) show the top displacement history of Pier 2 and Pier 3. The top displacement history of Pier 2 and Pier 3 is the same. They moved in-phase with slight residual displacements.

The corresponding maximum column drift is listed in Table 4. It is seen that all the three cases have the same demanding of largest pier maximum displacements, varying from 0.331% in the SMA model to 0.329% in the RC model, since the input ground displacements normal to the fault are the same, as shown in Figure 5b. When doubling the input, the peak drift is 0.684% in the SMA model to 0.588% in the RC model, respectively. Overall, it is seen that the response of

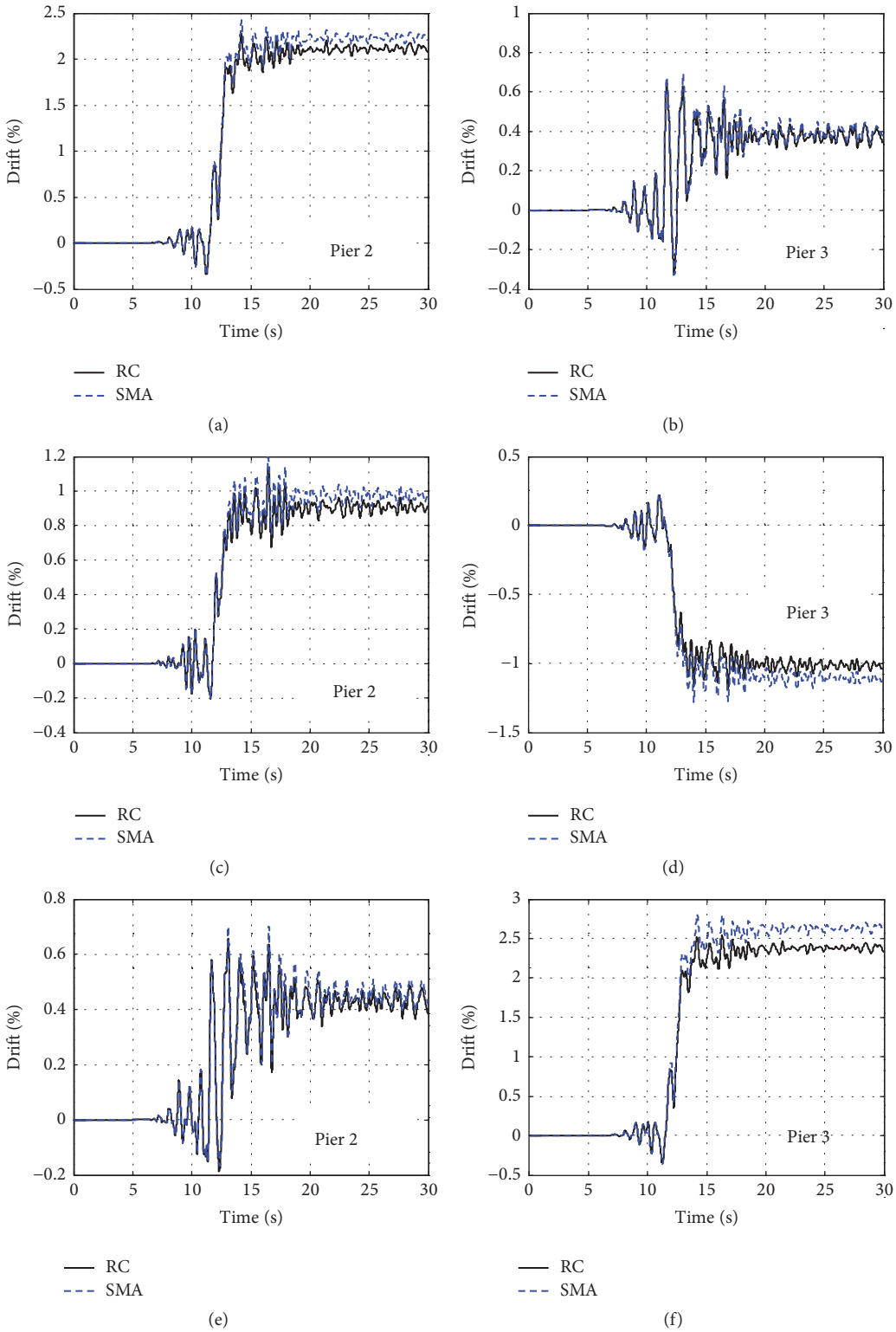

Figure 12: Displacement history of the top column: (a) Pier 2 in Case 1, (b) Pier 3 in Case 1, (c) Pier 2 in Case 2, (d) Pier 3 in Case 2, (e) Pier 2 in Case 3, and (f) Pier 3 in Case 3.

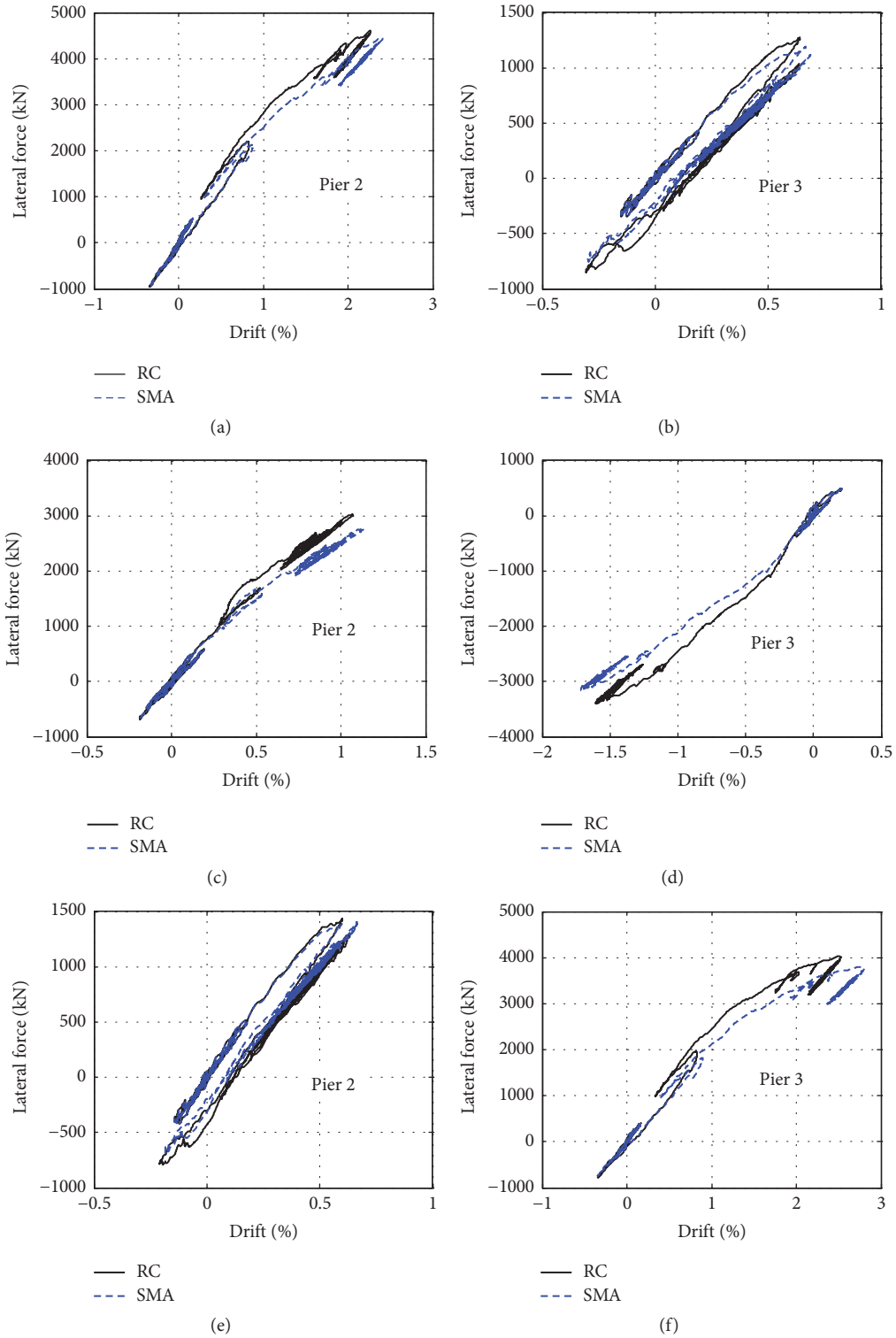

Figure 13: Calculated force displacement hysteresis of the column: (a) Pier 2 in Case 1, (b) Pier 3 in Case 1, (c) Pier 2 in Case 2, (d) Pier 3 in Case 2, (e) Pier 2 in Case 3, and (f) Pier 3 in Case 3.

Pier 2 and Pier 3 in the longitudinal is too small compared to the response in the transverse direction. That is because the displacement ground motion is like a single sinusoidal wave and the absence of high-frequency content.

According to the result mentioned in Table 4, the drift result of the piers in the longitudinal direction from the displacement excitation is relatively too small compared to the transverse direction. The fault-normal displacement time

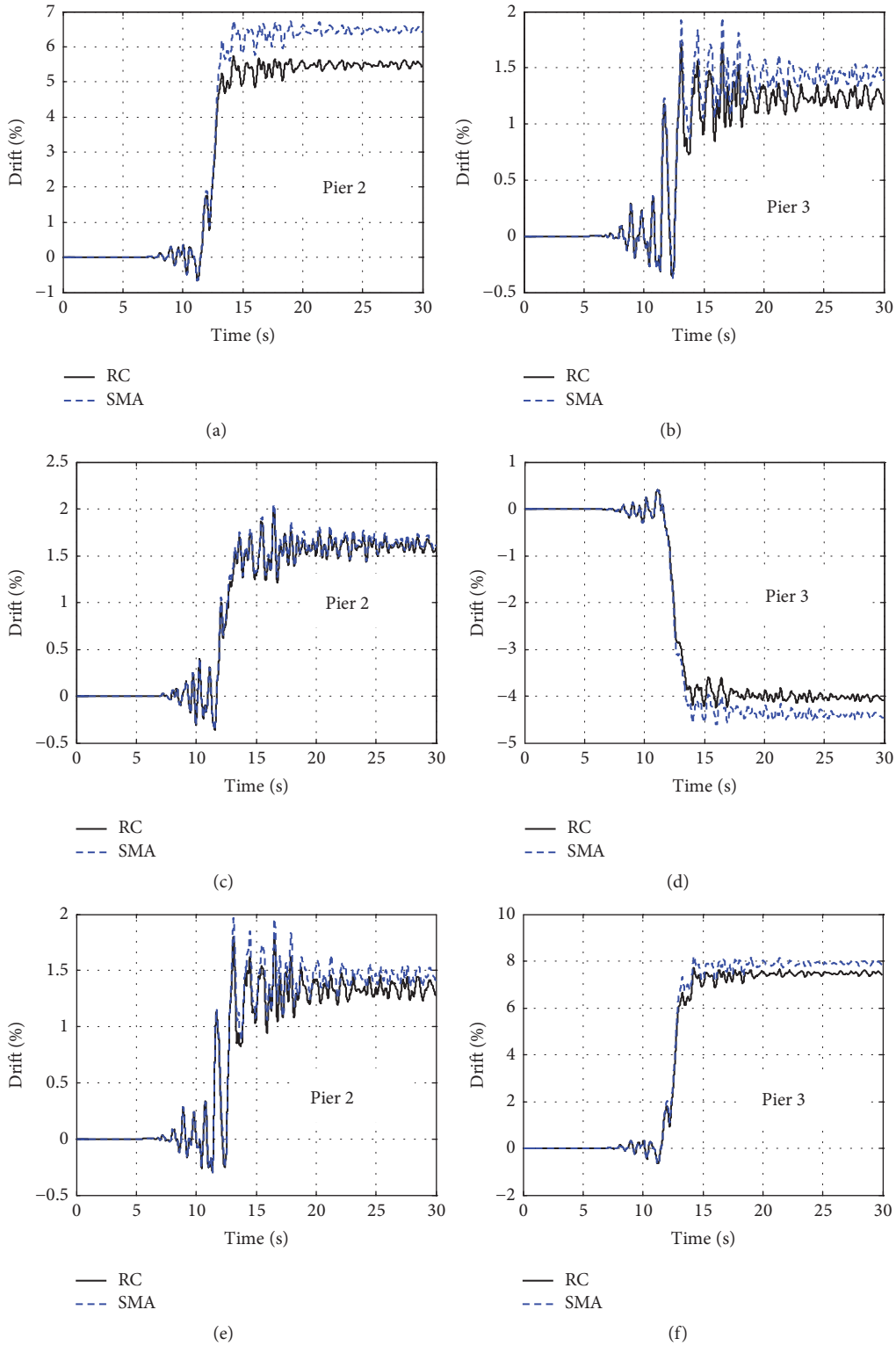

Figure 14: Displacement history of the top column with double amplified motions: (a) Pier 2 in Case 1, (b) Pier 3 in Case 1, (c) Pier 2 in Case 2, (d) Pier 3 in Case 2, (e) Pier 2 in Case 3, and (f) Pier 3 in Case 3.

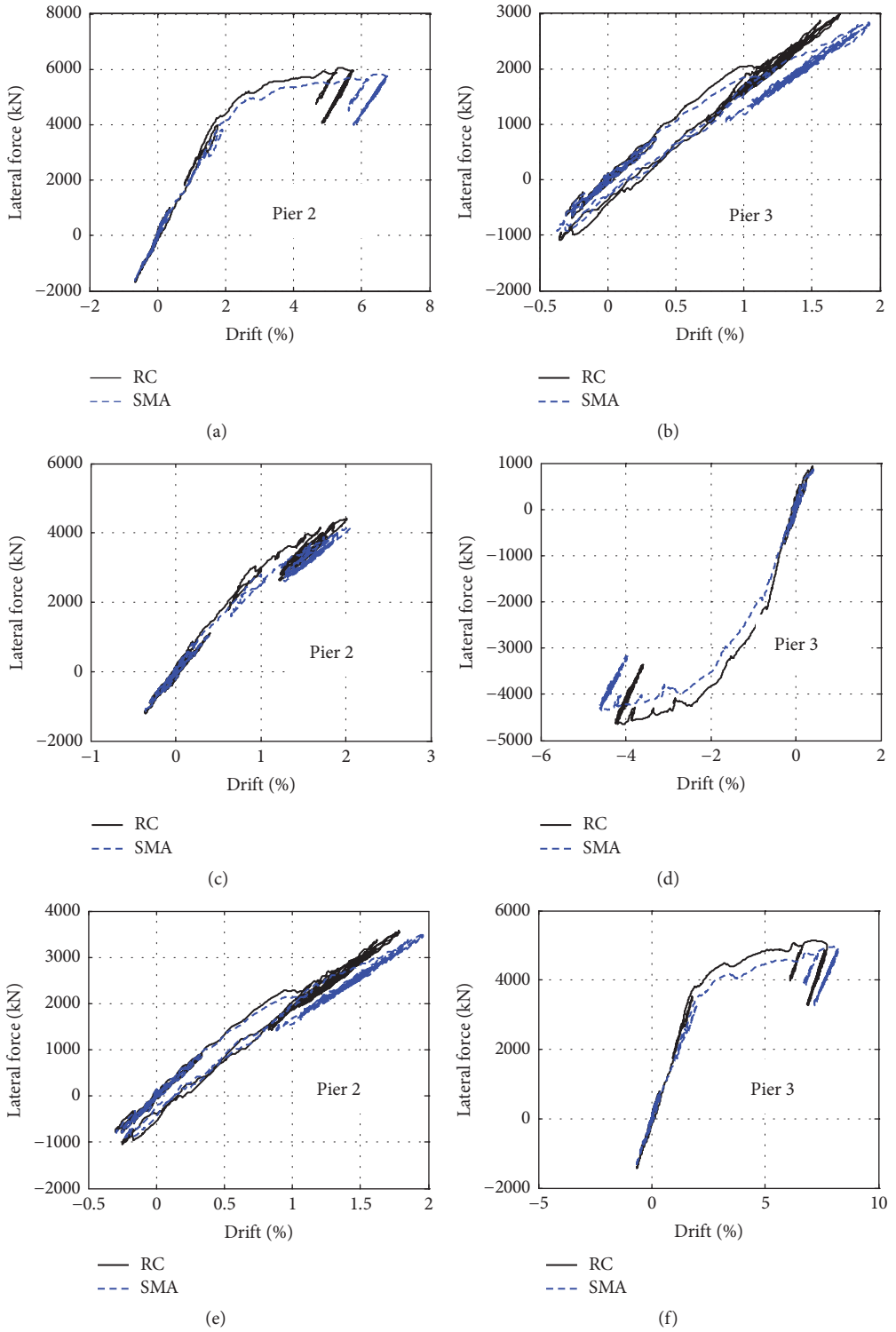

FIGURE 15: Calculated force displacement hysteresis of the column with double amplified motions: (a) Pier 2 in Case 1, (b) Pier 3 in Case 1, (c) Pier 2 in Case 2, (d) Pier 3 in Case 2, (e) Pier 2 in Case 3, and (f) Pier 3 in Case 3.

history is obtained through a double time-integration of the recorded acceleration history. So the uniform excitation in the longitudinal direction using the acceleration time history is compared with the excitation using the displacement records. The corresponding maximum column drift is listed in Table 5. For the acceleration excitation, the RC column had the peak drift of 2.40% and the SMA column had the peak drift of 3.25%. These results are comparable to the

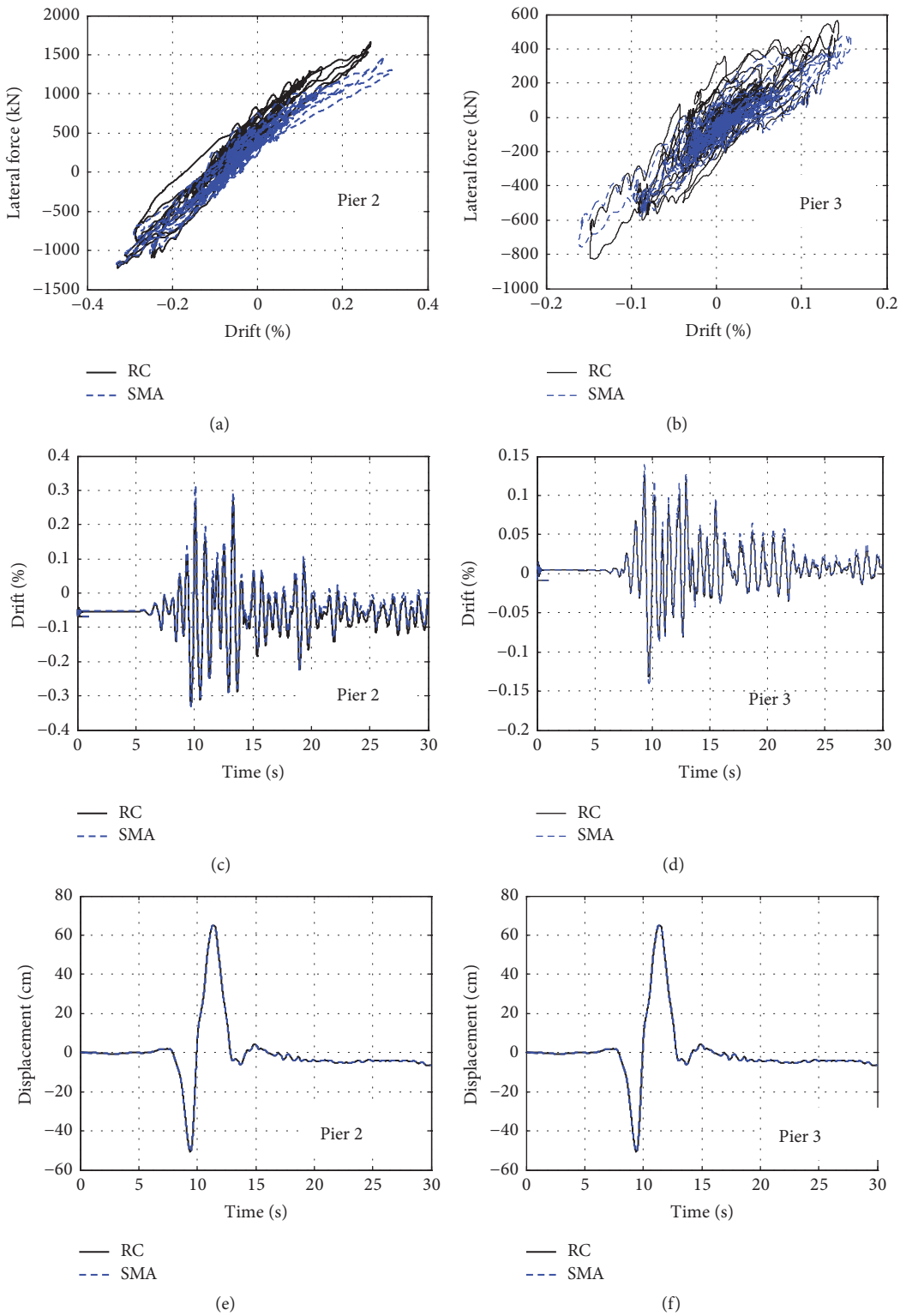

FIGURE 16: The response of Pier 2 and Pier 3 with full amplified motions: (a) and (b) base shear versus drift hysteresis curves; (c) and (d) relative drift of piers; (e) and (f) top displacement history of piers.

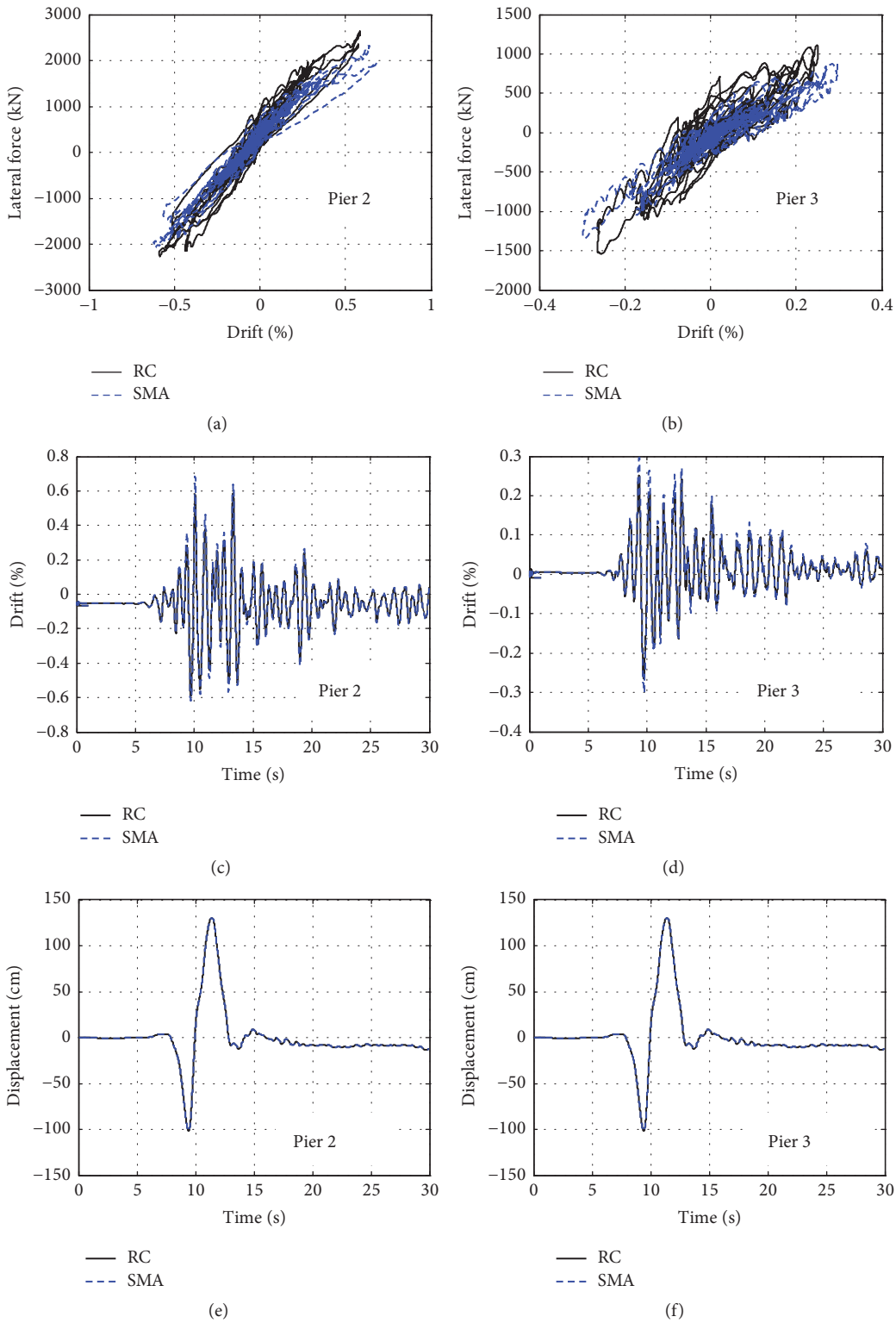

Figure 17: The response of Pier 2 and Pier 3 with double amplified motions: (a) and (b) base shear versus drift hysteresis curves; (c) and (d) relative drift of piers; (e) and (f) top displacement history of piers.

Table 4: Peak drift results of fault-rupture study in the longitudinal direction (%).

Case	Fault location	Model	Peak drift(%) Pier2/Pier3	Double input peak drift(%) Pier2/Pier3
Case 1	Abut.1 and Pier 2	SMA	0.331/0.143	0.684/0.299
		RC	0.329/0.131	0.588/0.265
Case 2	Pier2 and Pier3	SMA	0.331/0.143	0.684/0.299
		RC	0.329/0.131	0.588/0.265
Case 3	Pier3 and Abut.4	SMA	0.331/0.143	0.684/0.299
		RC	0.329/0.131	0.588/0.265

Table 5: Peak drift results of acceleration and displacement excitation in the longitudinal direction (%).

Case	Motion type	Model	Peak drift(%)	Double input peak drift(%)
1	Acceleration	SMA	3.25	11.57
		RC	2.40	10.85
2	Displacement	SMA	0.331	0.684
		RC	0.329	0.588

transverse direction, as expected in common sense. When double amplifying the amplitude of the acceleration ground motion, the RC column had the peak drift of 10.85% and the SMA column had the peak drift of 11.57%. So in the longitudinal direction analysis, the acceleration excitation should be used to get reasonable results.

5. Conclusions

The objective of this study is to assess the performance of columns that represent the SR99 Bridge piers to be built in Seattle, WA. The seismic response of three-span bridges with innovative materials under a near-fault ground motion with incoherent motions that included the fault-rupture effect was analyzed. Findings from analytical studies on the columns with plastic hinges detailed with SMA and ECC lead to the following conclusions.

(1) For the uniform displacement excitation, both the SMA column and the RC column have relatively smaller drift demand. The E55 motion causes the largest pier maximum displacements in the transverse direction, varying from 1.88 % in the SMA model to 1.70% in the RC model. The W18 motion is the most demanding of all three motions in the longitudinal direction, varying from 3.25 % in the SMA model to 2.40% in the RC model. The SMA column has the bigger maximum displacement than the RC column.

(2) The time history results subjected to full amplified ground motions analysis show that there is no significant residual displacement subjected to the acceleration excitation, both for the RC bridge and the SMA bridge. The time history results subjected to double amplified ground motions analysis show that, in general, the columns with plastic hinges detailed with SMA and ECC exhibit bigger peak drift and smaller residual drift compared with conventional RC columns. The superelastic characteristics of SMA bars minimize residual displacements in SMA-reinforced concrete columns. The combination of SMA and ECC is found to substantially reduce the earthquake damage compared with conventional RC.

(3) Fault-parallel near-fault earthquakes typically exhibit a static permanent ground displacement caused by the relative movement of the two sides of the fault. When the fault is located between piers, the pier shows a higher demand. The different loading pattern of the structure on the fault is a determining factor.

(4) In the transverse direction including fault-rupture, the bridge with SMA columns has a bigger maximum displacement and residual displacement compared to the bridge with RC columns because of the smaller stiffness of the SMA model. For Case 1 and Case 3, the pier near the fault has significant peak drift demands. For Case 2, the seismic responses for fault-rupture motions result in bigger demands on bridge columns in the piers. It can be seen that the location of fault-rupture also can be a determining factor.

(5) In the longitudinal direction, the response of the piers using the displacement time history is too small compared to the response in the transverse direction. That is because the displacement ground motion is like a single sinusoidal wave and the absence of high-frequency content. So, in the longitudinal direction response, the acceleration excitation should be used in the time history analysis to get the reasonable results. The amplitude results of the drift are quite different between the acceleration excitation and displacement excitation.

Conflicts of Interest

The authors declare that they have no conflicts of interest.

Acknowledgments

This research was funded by the Washington Department of Transportation (WashDOT) Contract no. GCB1341 through a grant from the Federal Highway Administration (FHWA) program on Innovative Bridge Research and Deployment (IBRD). Invaluable comments from Dr. Bijan Khaleghi and Mr. Jed Bingle of WashDOT were received. Additional funding was provided by Federal Highway Administration under Contract no. DTFH61-07-C-00031. The support of Dr. Philip Yen of FHWA is appreciated. The first author acknowledges the support provided by Shanghai Institute of Technology and the National Science Foundation of China under Research Grant no. 51408360 during his stay at University of Nevada, Reno.

References

[1] V. V. Bertero, S. A. Mahin, and R. A. Herrera, "Aseismic design implications of near-fault san fernando earthquake records," *Earthquake Engineering & Structural Dynamics*, vol. 6, no. 1, pp. 31–42, 1978.

[2] A. Pamuk, E. Kalkan, and H. I. Ling, "Structural and geotechnical impacts of surface rupture on highway structures during recent earthquakes in Turkey," *Soil Dynamics and Earthquake Engineering*, vol. 25, no. 7-10, pp. 581–589, 2005.

[3] J. Shen, M. H. Tsai, K. C. Chang, and G. C. Lee, "Performance of a seismically isolated bridge under near-fault earthquake ground motions," *ASCE Journal of Structural Engineering*, vol. 130, no. 6, pp. 861–868, 2004.

[4] P. C. Roussis, M. C. Constantinou, M. Erdik, E. Durukal, and M. Dicleli, "Assessment of performance of seismic isolation system of Bolu Viaduct," *Journal of Bridge Engineering*, vol. 8, no. 4, pp. 182–190, 2003.

[5] S. W. Park, H. Ghasemi, J. Shen, P. G. Somerville, W. P. Yen, and M. Yashinsky, "Simulation of the seismic performance of the Bolu Viaduct subjected to near-fault ground motions," *Earthquake Engineering & Structural Dynamics*, vol. 33, no. 13, pp. 1249–1270, 2004.

[6] H. Choi, M. Saiidi, and P. Somerville, "Effects of near-fault ground motion and fault-rupture on the seismic response of reinforced concrete bridges," Tech. Rep., Center for Civil Engineering Earthquake Research, Department of Civil and Environmental Engineering, University of Nevada, Reno, Nevada, USA, 2007, Report No. CCEER-07-06.

[7] N. Johnson, R. T. Ranf, M. S. Saiidi, D. Sanders, and M. Eberhard, "Seismic testing of a two-span reinforced concrete bridge," *Journal of Bridge Engineering*, vol. 13, no. 2, pp. 173–182, 2008.

[8] H. Wang, *A study of RC columns with shape-memory-alloy and engineered cementitious composites*, Dissertation, University of Nevada, 2004.

[9] M. S. Saiidi and H. Wang, "Exploratory study of seismic response of concrete columns with shape memory alloys reinforcement," *ACI Structural Journal*, vol. 103, no. 3, pp. 436–443, 2006.

[10] R. DesRoches and M. Delemont, "Seismic retrofit of simply supported bridges using shape memory alloys," *Engineering Structures*, vol. 24, no. 3, pp. 325–332, 2002.

[11] V. C. Li, "On engineered cementitious composites (ECC)—a review of the material and its applications," *Journal of Advanced Concrete Technology*, vol. 1, no. 3, pp. 215–230, 2003.

[12] C. A. Cruz Noguez and M. S. Saiidi, "Shake-table studies of a four-span bridge model with advanced materials," *Journal of Structural Engineering*, vol. 138, no. 2, pp. 183–192, 2012.

[13] C. A. Cruz Noguez and M. S. Saiidi, "Performance of advanced materials during earthquake loading tests of a bridge system," *Journal of Structural Engineering (United States)*, vol. 139, no. 1, pp. 134–154, 2013.

[14] B. Nakashoji and M. Saiidi, "Seismic performance of square nickel-titanium reinforced ecc columns with headed couplers," Tech. Rep., Center For Civil Engineering Earthquake Research, Department Of Civil and Environmental Engineering, University of Nevada, Reno, Nevada, USA, 2014, Report No. CCEER-14-05.

[15] P. G. Somerville, "Characterizing near fault ground motion for the design and evaluation of bridges," in *Proceedings of the Third National Conference and Workshop on Bridges and Highways*, Portland, Oregon, USA, 2002.

[16] P. Somerville, K. Irikura, R. Graves et al., "Characterizing crustal earthquake slip models for the prediction of strong ground motion," *Seismological Research Letters*, vol. 70, no. 1, pp. 59–80, 1999.

[17] F. McKenna and L. G. Fenves, "OpenSees manual (PEER Center)," http://OpenSees.berkeley.edu, 2001, [Accessed on May 15, 2017].

[18] J. P. Ge, M. Saiidi, and S. Varela, "Computational Studies on the Seismic Response of the State Route 99 Bridge in Seattle with SMA/ECC Plastic Hinges," *Frontiers of Structural and Civil Engineering*, pp. 1–16, 2018, https://doi.org/10.1007/s11709-018-0482-6.

[19] C. Chadwell and TRC., "XTRACT," Case 3.0.9, Single User, Educational, 2011.

[20] N. I. Wehbe, M. S. Saiidi, and D. H. Sanders, "Seismic performance of rectangular bridge columns with moderate confinement," *ACI Structural Journal*, vol. 96, no. 2, pp. 248–258, 1999.